Molecular Dynamics Studies on the Role of Tetramethylammonium Cations in the Stability of the Silica Octamers $Si_8O_{20}^{8-}$ in Solution

S. Caratzoulas,*,† D. G. Vlachos,† and M. Tsapatsis‡

Department of Chemical Engineering, University of Delaware, Newark, Delaware 19716 and Department of Chemical Engineering & Materials Science, University of Minnesota, 421 Washington Avenue SE, Minneapolis, Minnesota 55455

Received: January 6, 2005; In Final Form: March 24, 2005

The stability of silica octamers, $Si_8O_{20}^{8-}$ observed in tetramethylammonium (TMA) solutions by Kinrade et al. (*Inorg. Chem.* **1998**, *37*, 4272) is investigated in connection with the TMA concentration by performing equilibrium molecular dynamics simulations of $Si_8O_{20}^{8-}$−TMA−water mixture at two concentrations. At the experimental concentration at which the silica octamers have been observed spectroscopically, we find that, on the average, six TMA molecules surround the silica octamer, coordinated so that each cation occupies a face of the cubic octamer. We also find that upon TMA adsorption, water molecules associated with the siloxane oxygens leave the silica surface, whereas the hydrogen-bond network of the silanol oxygens with water molecules remains intact. No TMA adsorption is observed at the concentration at which the octamers have not been observed.

I. Introduction

The ability to fabricate complex, nanostructured materials tailored for specialized applications remains an elusive goal. An interesting strategy for such materials synthesis involves hierarchical assembly of supramolecular precursors to form complex organic−inorganic structures with crystalline order. One such example is pure silica zeolites, a class of materials of fundamental importance and with wide-ranging technological applications (catalysts,[1−3] separation membranes with nano- or subnano-scale molecular recognition and shape selectivity,[4−7] optical electronics,[8] bio-implants,[9−11] low-*k* dielectrics[12] etc.). The design of such synthetic procedures remains chiefly an empirical endeavor and usually requires very costly trial-and-error modifications to reagents and conditions. Hierarchical assembly and self-organization, in general, are two of the most complex problems because they appear to involve numerous simultaneous and interdependent equilibria and reactive (bond-formation or cleaving) steps. The complexity of the problem is such that the structures, fundamental principles, and mechanisms that control hierarchical assembly still elude us.

In zeolite crystallization under hydrothermal conditions, in particular, organic molecules such as amines or tetraalkylammonium (TAA) cations are being routinely used in the synthesis and production of most commercially important zeolites. Apart from the fact that the use of organocations can affect the rate at which a particular material is formed, it has long been accepted that their role is also one of structure direction, in the sense that they organize the framework formation around them and thereby determine the zeolite pore architecture; this has been the working hypothesis of computational studies in the past.[13,14] However, the exact atomistic-scale mechanisms of template-assisted formation of nanoporous or microporous, zeolite-type materials are still not understood. One of the reasons is that the nature and extent of the interactions between the organic and inorganic components in the growth medium, as well as their interactions with the solvent itself, remain to be elucidated. By gaining insight into the fundamentals of these interactions, not only shall we be able to compute important kinetic quantities such as growth rates, but we shall also be able to *influence* crystal structure and morphology by appropriate selection of template molecules.

There is substantial experimental evidence, by a multitude of experimental techniques, that small colloidal particles, 10 nm or less in diameter, are present during the synthesis of several zeolite types such as Si−MFI (silicalite-1), Si−MTW, Si−BEA, and LTA.[15−28] The consensus regarding the presence of these subcolloidal particles notwithstanding, little is known about their structure, their role in the growth process, their interactions, and the factors that determine their shape or size. The silica nanoparticles are bound to carry surface charge and possibly internal charge because of dangling $Si-O^-$ bonds. So, we expect the TAA cations to play the role of the counterions, namely, to get adsorbed at the negatively charged surfaces and form the so-called screening double layer. However, the hydrophobic character of the TAAs should not go unnoticed; it is very likely that they play a second, and not the least minor, role: to form a "shield" around the silicate nanoparticle that protects the siloxane (Si−O−Si) bonds from being attacked by water molecules.

There is experimental evidence supporting the idea of a TAA "shield" around the silica nanoparticles. While in TAA solutions the exchange of silica between these soluble species is slow (hours), the exchange rate in alkali−metal solutions is fast (seconds to minutes).[29−31] These differences in exchange rates point to relatively strongly bound TAA cations. Furthermore, Fedeyko et al. have recently investigated the nanoparticle formation and structure using conductivity, pH, and small-angle scattering methods.[32] Their studies show that the nanoparticles have a core−shell structure: silica in the core and TAA cations

* Author to whom correspondence should be addressed. E-mail: caratzou@che.Udel.edu.
† University of Delaware.
‡ University of Minnesota.

10.1021/jp0500891 CCC: $30.25
Published on Web 04/21/2005

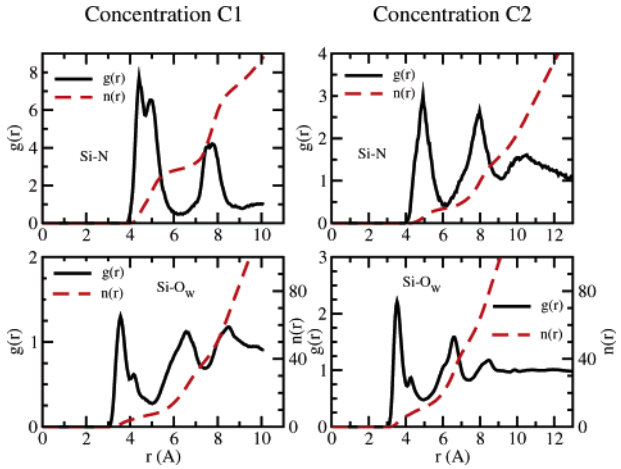

Figure 1. Atom−atom pair correlation functions for the molecular pairs silica octamer−TMA and silica octamer−water. The left panels refer to concentration C1; the right panels refer to C2. The upper panels refer to the pairs Si−N; the lower panels refer to the pairs Si−O_W, where O_W denotes water oxygen. Note that, in the lower panels, the running coordination numbers, $n_{\alpha\beta}(r)$, refer to the right-hand scales of the graphs. The correlation functions are shown in black; the running coordination numbers are shown in red.

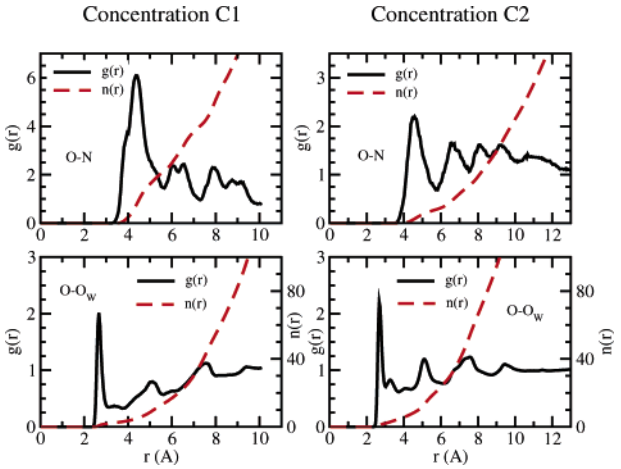

Figure 2. Atom−atom pair correlation functions for the molecular pairs silica octamer−TMA and silica octamer−water. The left panels refer to concentration C1; the right panels refer to C2. The upper panels refer to the pairs O−N; the lower panels refer to the pairs O−O_W, where O_W denotes water oxygen. Note that, in the lower panels, the running coordination numbers, $n_{\alpha\beta}(r)$, refer to the right-hand scales of the graphs. (Color coding same as in Figure 1.)

in the shell. However, their work does not reveal any more details on the structure of these silica−TAA "assemblies," namely, TAA coordination numbers or coordination geometry.

In this article, we attempt to provide answers to questions that pertain to the structural aspects of the problem. To that end, we focus our attention to a smaller scale system: well-defined silica clusters that have been identified spectroscopically (^{29}Si NMR) by Knight and co-workers. Despite the subnanoscale dimensions, these systems already manifest clear signs of control over speciation. Specifically, and as opposed to the multitude of small, often asymmetrical silicate anions found in alkali−metal silicate solutions,[33−36] concentrated tetramethylammonium (TMA) silicates are dominated by a few compact, cagelike species such as the cubic octamer $Si_8O_{20}^{-8}$ (or "double four-ring," Q_8^3) and to a lesser extent the prismatic hexamer (or "double three-ring," Q_6^3).[30] In particular, for solutions containing 2.00 mol/kg TMAOH and 0.25−1.00 mol/kg SiO_2, the ^{29}Si NMR peak that Kinrade et al. have assigned to the cubic octamer, Q_8^3, increases in intensity with SiO_2 concentration (see Figure 2 in ref 30).

To account for the formation of Q_8^3, Kinrade et al. have proposed the following reaction equilibria:

$$8H_3SiO_4^- + xTMA^+ \rightleftarrows [Si_8O_{20}\cdot xTMA]^{(8-x)-} + 12H_2O$$

For an [OH^-]:[Si] ratio of 1:1 or more, analysis of their NMR data reveals that $x = 8 \pm 1$.[30] Naturally, this result is in accordance with charge balance considerations but does not provide any structural information, namely, TMA coordination numbers or geometry. Furthermore, in our view, the solvent structure in the vicinity of the silica solutes is a critical issue that must be addressed and elucidated to understand the reasons that lead to the stability of these species, especially in view of the fact that the screening double layer consists of charged organic molecules, whose hydrophobic alkyl chains may influence the local structure of the solvent. As we mentioned before, very little consensus among experimentalists exists regarding these questions. Controversy arises primarily because the techniques that are used, such as NMR and neutron scattering as well as X-ray scattering, are either not sensitive to the detailed microscopic structure or else require a considerable degree of interpretation to obtain structural information.

We have chosen to perform atomistic-level molecular dynamics (MD) simulations to investigate these issues. In this article, we report on such calculations in $Si_8O_{20}^{8-}$−TMA−water mixtures at two concentrations: one at $1Si_8O_{20}^{8-}$:16TMA:450H_2O, corresponding to the maximum silica to TMA ratio used by Kinrade et al. in their NMR experiments, namely, 2.0 mol/kg TMA:1.0 mol/kg SiO_2; and the other at $1Si_8O_{20}^{8-}$:8TMA:670H_2O, namely, 0.66 mol/kg TMA:0.66 mol/kg SiO_2, corresponding to a dilute solution in which cubic octamers have *not* been observed. Hereinafter, we shall be referring to these two concentration conditions as C1 and C2, respectively. Our objectives here are to investigate on one hand trends with dilution and on the other the hypothesis that one of the roles of TMA is to form a protective shield around the silica polyion against hydrolysis.

II. Force Field and Method

The force field for intermolecular interactions was based on pairwise additive potentials between atomic sites:

$$u_{\alpha\beta}(r) = \frac{q_\alpha q_\beta}{r} + 4\epsilon_{\alpha\beta}\left[\left(\frac{\sigma_{\alpha\beta}}{r}\right)^6 - \left(\frac{\sigma_{\alpha\beta}}{r}\right)^{12}\right] \qquad (1)$$

where α and β denote a pair of interacting sites on different molecules, r is the separation between two interacting sites, q_α is the point charge at site α, and $\epsilon_{\alpha\beta}$, $\sigma_{\alpha\beta}$ are, respectively, the energy and distance parameters in the Lennard-Jones potential.[37]

For water molecules, we have used the parameter values in the TIPS3P model of Jorgensen.[38] The silica octamer and TMA Lennard-Jones parameters we used in this study are given in Table 1. For cross-species interactions, the relevant Lennard-Jones parameters were obtained by the Lorentz−Berthelot rule[37]

$$\sigma_{\alpha\beta} = \frac{1}{2}(\sigma_{\alpha\alpha} + \sigma_{\beta\beta}),\ \epsilon_{\alpha\beta} = (\epsilon_{\alpha\alpha}\epsilon_{\beta\beta})^{1/2} \qquad (2)$$

All partial charges have been obtained by ab initio calculations at the same theory level for all solute molecules. In particular, the partial charges for the TMA molecule we have taken from the literature.[39] For the silicate octamer, we

TABLE 1: Intermolecular Potential Parameters

	ϵ (kcal/mol)	σ (Å)	q
Water (TIPS3P, Reference 38)			
oxygen	0.1521	3.1501	−0.834
hydrogen	0.0	0.0	0.417
Tetramethylammonium (TMA)			
nitrogen	0.17	3.25	0.288757
carbon		3.29	−0.301576
hydrogen	0.02	1.78	0.1604
Silica Octamer ($Si_8O_{20}^{8-}$)			
silicon	0.04	4.0534	1.550198
siloxane oxygen	0.105	3.35	−0.874786
silanol oxygen	0.105	3.35	−1.227322

performed ab initio calculations at the Hartree−Fock level with 6−31*G*(*d*) basis, while the self-consistent isodensity polarizable continuum model (SCIPCM)[40] was employed to take the water solvent into account; partial charges were subsequently obtained using the CHelpG[41] scheme as implemented by *Gaussian.*[42] The partial charges for all the molecules are given in Table 1.

All types of molecules in our simulations were held rigid. Specifically, for both the octamer and the TMA molecules, we adopted configurations that had previously been optimized in vacuo by ab initio methods.[42] For the geometry of the water molecules, we have taken the bond lengths equal to 0.9573 Å and the bond angle equal to 104.52°.

In the simulation for the concentration C1, the simulation box contained 1 cubic octamer ($Si_8O_{20}^{8-}$), 16 TMA molecules, 450 water molecules, and 8 OH^- ions for electroneutrality. To obtain a starting configuration, one silica octamer along with 16 TMA molecules and 8 hydroxyl ions were optimized in vacuo and the whole "assembly" was subsequently placed in a water cavity at the center of a cubic simulation box of lattice constant 23.760 Å. The system was then optimized to remove accidental overlaps between interaction sites. The simulation extended up to 500 ps, of which the first 250 ps were the equilibration phase.

In the simulation for the concentration C2, the simulation box contained 1 cubic octamer ($Si_8O_{20}^{8-}$), 8 TMA molecules, and 670 water molecules. The starting configuration was prepared in a fashion similar to that for C1, in a cubic simulation box of lattice constant 27.318 Å. Because of the low concentrations involved, and the relatively larger simulation box, this simulation was extended up to 1.0 ns, of which the first 500 ps consisted of the equilibration phase of the dynamics.

We performed the MD simulations using periodic boundary conditions in the *NVT* ensemble at $T = 300$ K with a Nosé−Hoover thermostat. The equations of motion were integrated using the Verlet algorithm, and bond constraints for the rigid molecules were enforced using the SHAKE algorithm.[37,43] A time step of 1 fs was adequate to satisfy energy conservation in both cases. For the short-range forces, we employed the minimum image convention, and for the long-range electrostatic forces, we used the Ewald summation.[37,43]

The DL_POLY parallel molecular dynamics simulation package developed at Daresbury Laboratory, U.K., was used.[44]

III. Results

Atom−atom pair correlation functions $g_{\alpha\beta}(r)$ provide a very good method to obtain structural information. In Figures 1 and 2, we display the atom−atom pair correlation functions and corresponding running coordination numbers

$$n_{\alpha\beta}(r) = 4\pi\rho_\beta \int_0^r g_{\alpha\beta}(r')\, r'^2\, dr' \qquad (3)$$

where ρ_β is the bulk number density of atom β, for the molecular pairs silica octamer−TMA, and silica octamer−water, for the two concentrations C1 and C2.

We observe significant differences between the two concentrations. From Figure 1 (upper panels), in the case of the concentrated solution (C1), there are on the average 2.9 nitrogen atoms around each Si atom within a radius of 6.5 Å. Because each Si atom is shared by three faces in the cubic octamer, and because the system is isotropic, we infer that, on the average, the silica octamer is surrounded by approximately 6 TMA molecules. The presence of a near plateau in the running coordination number of the TMA nitrogen atoms manifests the presence of a distinct TMA coordination shell around the silica octamer. In stark contrast, in the case of the dilute solution (C2), we find that only 0.4 nitrogen atoms are on the average within 6.2 Å of each Si atom, which is roughly equivalent to one TMA molecule per cube.

Elementary arguments on the electrostatics and stability of interacting charged species suggest that a TMA cation upon adsorption should occupy a face of the cubic octamer. Thus, on the basis of the coordination number deduced from the first peak in $g_{SiN}(r)$ above, we propose a facial coordination of the TMA cations around the silica octamer, which, at full coverage of the octamer, results in octahedral geometry. Let a denote the nearest Si−Si separation in the cubic octamer and d denote the distance of the adsorbed TMA molecule from the plane defined by the Si atoms in the face that TMA occupies. For $a \approx 3.23$ Å (obtained from the optimized geometry for the octamer in gas phase) and the peak at 4.5 Å in $g_{SiN}(r)$, and *assuming* that the TMA center of mass lies in the cube's symmetry axis normal to the corresponding face, we obtain $d \approx 3.83$ Å. Then, for the proposed octahedral geometry, a trivial calculation predicts a second peak in $g_{SiN}(r)$ at $r = \sqrt{3a^2/2 + d^2 + 2ad}$, which in this case gives about 7.5 Å. Indeed, the second peak in $g_{SiN}(r)$ (Figure 1, upper-left panel) is located at about 7.7 Å, in very good agreement with the proposed geometry.

The facial coordination of TMA around the silica octamer, as suggested by the Si−N pair distribution function above, is also consistent with the octamer O−N pair distribution function shown in Figure 2. Indispensably, the TMA coordination inferred from our simulations is in quantitative agreement with the findings of Wiebcke and Hoebbel for the crystal structure of $[NMe_4]_{16}[Si_8O_{20}][OH]_8 \cdot 116H_2O$;[45] and Wiebcke et al. in the determination of the crystal structure of $[N(CH_3)_4]_8[Si_8O_{20}] \cdot 65H_2O$ by single-crystal X-ray diffraction and variable-temperature MAS NMR spectroscopy.[46]

It is interesting to look at the solvent structure around the silica solute. The main peak in the Si−O_W pair distribution function (Figure 1, lower panels) is at the same location both in C1 and C2, but there is a much stronger association between Si and water in the case of the dilute solution. There are on the average 7.3 water molecules within 5.0 Å of each Si atom in C1, compared to 12 for C2 within the same radius. Evidently, TMA adsorption onto the faces of the octamer causes the solvent molecules in the vicinity of the silica solute to reorganize. Here, the water molecules in the vicinity of the octamer move out of the way as the TMA molecules approach the surface. The solvent reorganization in the case of the concentrated solution (C1) is more evident in Figure 3, where we display $g_{SiOW}(r)$ for silica octamer−water mixture in the *absence* of TMA. There is practically no difference between C2 and the TMA-free solution. In view of the previous analysis, which showed that practically no TMA adsorption takes place in the case of the dilute solution, this result was anticipated.

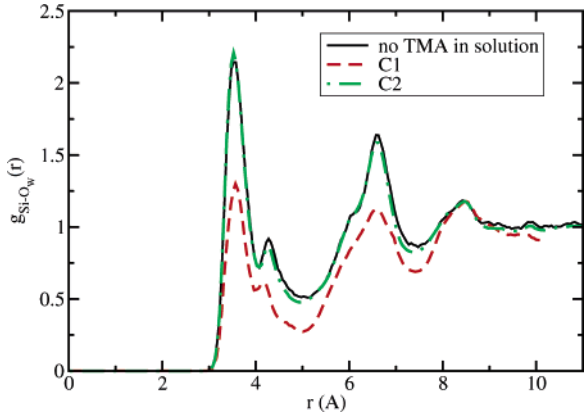

Figure 3. Pair distribution function for the pair Si−O_W in silica octamer−water mixture in the absence of TMA (black, solid line). For the sake of comparison, we also display the corresponding pair distribution functions for the solutions with concentrations C1 (red, dashed line) and C2 (green, dashed−dotted line). Notice that there are practically no differences between the TMA-free solution and the dilute solution (C2).

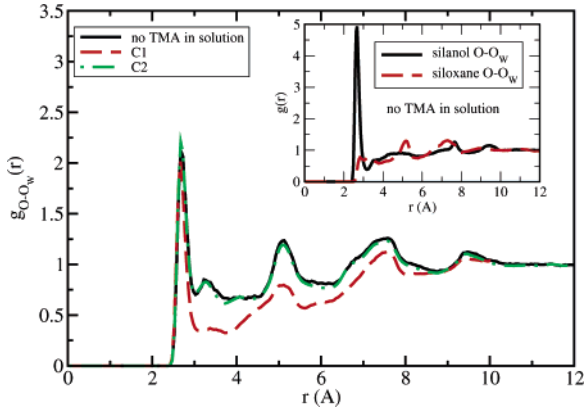

Figure 4. Pair distribution function for the pair O−O_W in silica octamer−water mixture in the absence of TMA (black, solid line). For the sake of comparison, we also display the pair distribution functions for the solutions with concentrations C1 (red, dashed line) and C2 (green, dashed−dotted line). Notice that there are practically no differences between the TMA-free solution (black line) and the C2 solution (green line). Inset: we display the silanol oxygen−water oxygen (black, solid line) and siloxane oxygen−water oxygen (red, dashed line) *individual* contributions to the $g_{OO_W}(r)$ for TMA-free solution. Notice that the main peak at 2.7 Å in $g_{OO_W}(r)$ is almost entirely due to the silanol oxygens. Similar curves are obtained for the solutions with concentrations C1 and C2.

However, this is half the story because clearly TMA adsorption, even in the case of the concentrated solution, does not expel all the solvent molecules from the surface of the octamer. The lower panels in Figure 2 show the O−O_W pair distribution functions for the two concentrations C1 and C2. In both, the first peak occurs at approximately the *optimum hydrogen bond distance* of 2.7 Å, and it corresponds very closely to $g_{O_WO_W}(r)$ for pure TIPS3P water (not shown here). Analysis shows that the main peak in $g_{OO_W}(r)$ is almost entirely due to the silanol oxygens (Si−O^-) (see inset in Figure 4 and Figure 5). Let O_h and O_x denote respectively silanol and siloxane oxygens. For the concentrated solution (C1), the distribution $g_{O_hO_W}(r)$ (shown in Figure 5) demonstrates that 3.0 water molecules are on the average within 2.7 Å of each O_h atom, in agreement with the experiments of Wiebcke et al.[46,47] From $g_{O_xO_W}(r)$, we have 0.2 neighboring water molecules within 3.0 Å of each O_x atom. For TMA-free solution, these numbers are 3.0 and 1.2, respectively. So, the differences seen in the silica oxygen−water

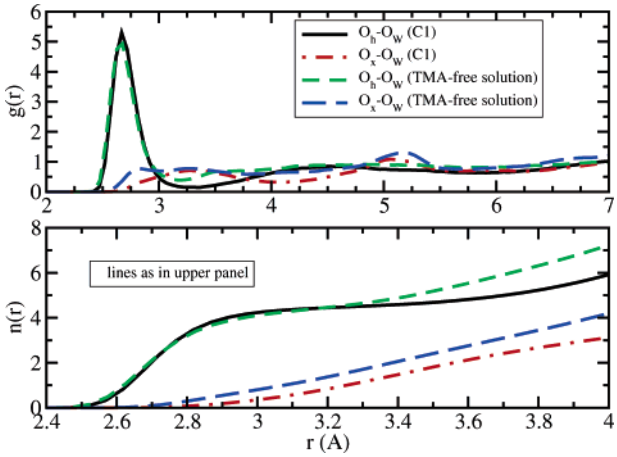

Figure 5. Upper panel: the pair distribution function $g_{OO_W}(r)$ for the solution with concentration C1, shown in red in Figure 4, is analyzed here in individual contributions $g_{O_hO_W}(r)$ (black, solid line) and $g_{O_xO_W}(r)$ (red, dotted-dashed line), where O_h, O_x denote silanol and siloxane oxygens, respectively. The respective distributions for the TMA-free solution (inset of Figure 4) are also displayed for the sake of comparison (green, short-dashed and blue, long-dashed lines, respectively). Lower panel: the running coordination numbers of the distributions displayed in the upper panel, for the range between 2.4 and 4.0 Å.

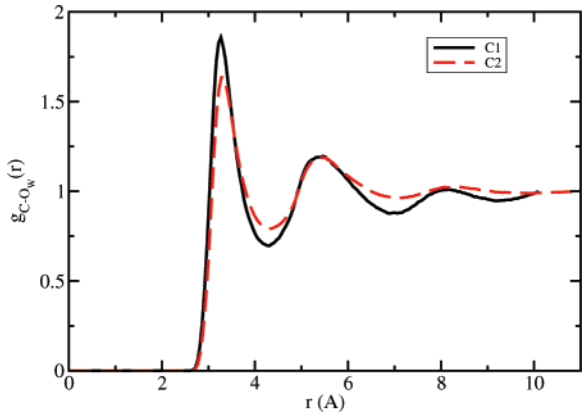

Figure 6. TMA carbon−water oxygen pair correlation function for both concentrations considered, C1 (black, solid line) and C2 (red, dashed line).

oxygen distributions of Figure 4 between the concentrated solution and the TMA-free solution are due to water molecules in the vicinity of the siloxane oxygens, possibly hydrogen-bonded to them, leaving the silica surface (approximately one water molecule per oxygen bridge) upon TMA adsorption. On the other hand, the solvent structure in the vicinity of the silanol oxygens does *not* appear to be affected by the presence of TMA molecules at the surface of the octamer. By carrying out the same analysis for the dilute solution (C2), we obtain exactly the same number of water molecules neighboring silanol or siloxane oxygens.

In Figure 6, we display the pair distribution function g_{CO_W}(r), where C denotes the TMA methyl group carbon atom, for both concentrations considered here. Both distributions are typical of a methyl group in a polar medium, clearly indicating the formation of a hydration sphere around it. We find that the first hydration shell, in both cases, includes on the average about 8 water molecules, but a more accurate number of the overall number of water molecules in the first TMA hydration shell is provided by $g_{NO_W}(r)$ (not shown), upon integration of which we find on the average about 23.5 water molecules within 5.5 Å of each N atom.

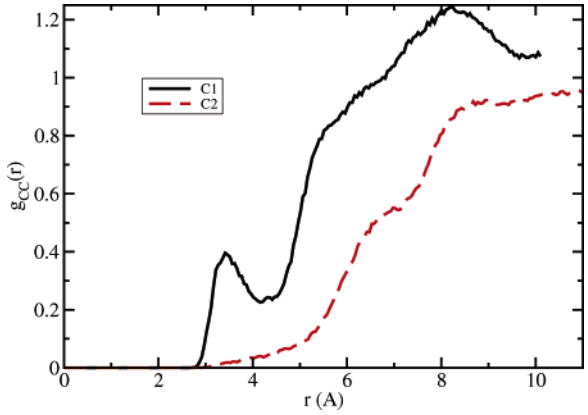

Figure 7. Carbon−carbon pair correlation function for both concentrations considered, C1 (black, solid line) and C2 (red, dashed line).

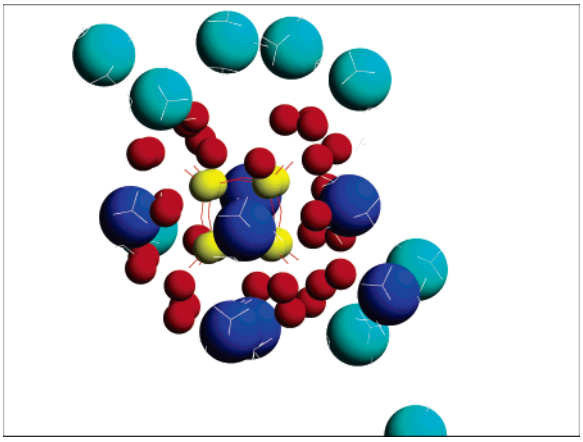

Figure 8. Representative configuration in the vicinity of the silica octamer from the simulation at concentration C1. Color coding: Si atoms, yellow balls; water oxygen, red balls; TMA nitrogen atoms within a radius of 6.5 Å of Si atoms, blue balls; rest of TMA nitrogen atoms, cyan balls (radii not drawn to scale).

Of interest is also the carbon−carbon distribution function, $g_{CC}(r)$, shown in Figure 7 for both C1 and C2. In the case of the dilute solution (C2, red, dashed line), and despite their hydrophobic character, we see that there is no association among the TMA molecules. Their motions are, of course, highly correlated, as indicated by the tail of the distribution; the long-range Coulomb interactions clearly dictate the dynamics and lead to the depicted behavior. One obtains the same picture in the case of the solution C1 (black, solid line), with the exception of the short peak at ~3.5 Å, which is due to the partial TMA ordering induced by the adsorption onto the silica surface. Note that the two peaks in $g_{SiN}(r)$ (upper-left panel in Figure 1) are about 3.3 Å apart. It is clear that at both concentrations examined in this article, there is no hydrophobic association among the TMA cations and their dynamical behavior is dictated primarily by electrostatics.

IV. Concluding Remarks

We have performed equilibrium molecular dynamics simulations of $Si_8O_{20}^{8-}$−TMA−water mixture at two different concentrations, C1 ($1Si_8O_{20}^{8-}$:16 TMA:450 H_2O) and C2 ($1Si_8O_{20}^{8-}$:8TMA:670H_2O). Definite concentration trends have been identified, having to do with TMA adsorption on the surface of the cubic octamer and concomitant water expulsion from the vicinity of the siloxane oxygens in the case of high TMA concentrations.

The following picture emerges. For the concentration C1, in which Kinrade et al. have observed the formation of the silica octamers Q_8^3, our MD simulations show that six TMA molecules on the average coordinate around the octamer. This distinct coordination shell has a more or less symmetric geometry, whereby each of the "adsorbed" cations occupies a face of the cubic surface (see Figure 8). By following the motion of each TMA molecule, we find that those molecules that were initially closer to the surface of the octamer (due to the gas phase optimization) are not necessarily those that are finally found to be strongly associated with the octamer. Indeed, a dynamic equilibrium is established, whereby TMA molecules get in and out of the octamer surface, often swapping positions with nearby TMA molecules. As TMA adsorbs, it expels water molecules from the surface of the octamer, but it appears to do so in a fashion that does *not* disrupt the hydrogen-bond network in which the silanol oxygens participate. The water molecules that leave the surface upon TMA adsorption are those previously found in the vicinity of the siloxane oxygens, which themselves participate in hydrogen bonds because of the negative partial charge that they carry, albeit smaller than that of the silanol oxygens (see Table 1). On the other hand, in the significantly more dilute solution (C2), where no octamers have been observed experimentally, our simulations show that practically no TMA adsorption takes place. Moreover, in this case, the solvent structure in the vicinity of the silica solute remains unaltered and in essence the same one we calculate for TMA-free solution.

Thus, our results suggest that there exists a very strong correlation between the thermodynamic stability of the octamers and the adsorption of TMA with concomitant water expulsion from the surface of the octamer. This strong correlation appears to lend credence to the theory that adsorption of TMA at the surface of the cubic octamer *protects* the siloxane group from hydrolysis by expelling water in the vicinity of the siloxane oxygens.[30,31] Although the role of the solvent in zeolite synthesis remains enigmatic, it is becoming clear that it is an important one and more work is needed in this direction. Past computational studies on the function of TAAs have routinely suppressed or overlooked the solvent effects and treated TAAs merely as counterions that primarily effect structure direction.[13,14] Our results strongly suggest that the two problems should be investigated in conjunction, not only because the water molecules can actively participate in the formation of clathrates,[45,46] but also because solvation effects can have a profound effect in the energetics of the underlying processes. For instance, the fact that, at the length scales considered in this study, the solvent tends to maintain its hydrogen-bond network with the silanol oxygens indicates that the solvent reorganization in consequence of TMA adsorption should result in an entropic cost in addition to the enthalpic one because of the removal of surface water previously H-bonded to the siloxane oxygens. Upon adsorption, similar solvent reorganization should be expected for the TMA solvation shell. Such considerations may affect the energetics and dynamics of the formation or stabilization of polysilicate−TAA complexes or nanoparticles and should not be neglected. For example, the preferential stabilization of the cubic octamer (Q_8^3) versus the prismatic hexamer (Q_6^3) may not be explained by gas phase considerations alone. A measure of the thermodynamic driving force for this preferential stabilization is the relative change in the free energies of formation $\Delta\Delta G_f^{(l)} = \Delta G_f^{(l)}(Q_8^3 \cdot nTMA) - \Delta G_f^{(l)}(Q_6^3 \cdot mTMA)$, where $\Delta G_f^{(l)}$ denotes the

free energy of formation in liquid phase. It is a simple matter to see that

$$\Delta\,\Delta G_f^{(l)} = \Delta\,\Delta G_f^{(g)} + [\Delta G_{sol}(Q_8^3 \cdot nTMA) - \Delta G_{sol}(Q_6^3 \cdot m\mathrm{TMA})] - [\Delta G_{sol}(Q_8^3) - \Delta G_{sol}(Q_6^3)] - (n-m)\Delta G_{sol}(\mathrm{TMA})$$

where $\Delta\,\Delta G_f^{(g)}$ is defined similarly to $\Delta\,\Delta G_f^{(l)}$ but in the gas phase, and ΔG_{sol} denotes solvation free-energy change. Solvation energy depends on solute geometry as well as on solvent structure in the vicinity of the former.

Returning to the dependence of the cubic octamer's stability on TMA concentration, it raises an important question: What is the underlying reason for the observed changes in TMA adsorption with concentration? Can the increased degree of TMA coordination around the silica octamer at high relative concentrations be simply ascribed to the entropy increase because of the higher TMA concentration? Or is it that the hydrogen bond dynamics, and thus the solvent structure in the vicinity of the silica solute, ultimately determine the lifetime of the silica−TMA assembly? We are currently investigating these issues.

Acknowledgment. Funding for this work was provided by NSF/NIRT (CTS-0103010) and NASAMicrogravity (98 HEDS-05-218). S.C. and D.G.V. gratefully acknowledge stimulating discussions with Professor Raul Lobo.

References and Notes

(1) Degnan, T. F. *Top. Catal.* **2000**, *13*, 349−356.
(2) Degnan, T. F. *J. Catal.* **2003**, *216*, 32−46.
(3) Joy, A.; Ramamurthy, V. *Chem.—Eur. J.* **2000**, *6*, 1287−1293.
(4) Hedlund, J. *J. Porous Mater.* **2000**, *7*, 455−464.
(5) Yan, Y.; Davis, M. E.; Gavalas, G. R. *Ind. Eng. Chem. Res.* **1995**, *34*, 1652−1661.
(6) Funke, H. H.; Argo, A. M.; Falconer, J. L.; Noble, R. D. *Ind. Eng. Chem. Res.* **1997**, *36*, 137−143.
(7) Lai, Z.; Bonilla, G.; Nery, G.; Diaz-Carretero, I.; Sujaoti, K.; Amat, M. A.; Kokkoli, E.; Terasaki, O.; Thompson, R. W.; Tsapatsis, M.; Vlachos, D. G. *Science* **2003**, *300*, 456−460.
(8) Wada, Y.; Okubo, T.; Ryo, M.; Nakazawa, T.; Hasegawa, Y.; Yanagida, S. *J. Am. Chem. Soc.* **2000**, *122*, 8583−8584.
(9) Beall, G. H. In *Mineralogical Society of America*; Heany, P. J., Prewitt, C. T., Gibbs, G. V., Eds.; Mineralogical Society of America: Washington, DC, 1994; pp 469−505.
(10) Davis, M. E.; Lobo, R. F. *Chem. Mater.* **1992**, *4*, 756−768.
(11) Zones, S. I.; Davis, M. E. *Curr. Opin. Solid State Mater. Sci.* **1996**, *1*, 107−117.
(12) Wang, Z.; Mitra, A.; Wang, H.; Huang, L.; Yan, Y. *Adv. Mater.* **2001**, *13*, 1463−1466.
(13) Lewis, D.; Willock, D.; Catlow, C.; Thomas, J. M.; Hutchings, G. *Nature* **1996**, *382*, 604.
(14) den Ouden, C.; Datema, K.; Visser, F.; Mackay, M.; Post, M. *Zeolites* **1991**, *11*, 418−424.
(15) Schoeman, B. J.; Sterte, J.; Otterstedt, J. E. *Zeolites* **1994**, *14*, 110−116.
(16) Schoeman, B. J.; Regev, O. *Zeolites* **1996**, *17*, 447−456.
(17) Schoeman, B. J. *Zeolites* **1997**, *18*, 97−105.
(18) Schoeman, B. J. *Microporous Mesoporous Mater.* **1998**, *22*, 9−22.
(19) Schoeman, B. J.; Higberg, K.; Sterte, J. *Nanostruct. Mater.* **1999**, *12*, 49−54.
(20) Kirschhock, C. E. A.; Ravishankar, R.; Jacobs, P. A.; Martens, J. A. *J. Phys. Chem. B* **1999**, *103*, 11021−11027.
(21) Kirschhock, C. E. A.; Ravishankar, R.; Verspeurt, F.; Grobet, P. J.; Jacobs, P. A.; Martens, J. A. *J. Phys. Chem. B* **1999**, *103*, 4965−4971.
(22) Kirschhock, C. E. A.; Ravishankar, R.; Van Looveren, L.; Jacobs, P. A.; Martens, J. A. *J. Phys. Chem. B* **1999**, *103*, 4972−4978.
(23) Mintova, S.; Olson, N. H.; Valtchev, V.; Bein, T. *Science* **1999**, *283*, 958−960.
(24) Ravishankar, R.; Kirschhock, C.; Schoeman, B. J.; Vanoppen, P.; Grobet, P. J.; Storck, S.; Maier, W. F.; Martens, J. A.; Schryver, F. C. D.; Jacobs, P. A. *J. Phys. Chem. B* **1998**, *102*, 2633−2639.
(25) Ravishankar, R.; Kirschhock, C. E. A.; Knops-Gerrits, P. P.; Feijen, E. J. P.; Grobet, P. J.; Vanoppen, P.; Schryver, F. C. D.; Miehe, G.; Fuess, H.; Schoeman, B. J.; Jacobs, P. A.; Martens, J. A. *J. Phys. Chem. B* **1999**, *103*, 4960−4964.
(26) Nikolakis, V.; Kokkoli, E.; Tirrell, M.; Tsapatsis, M.; Vlachos, D. *Chem. Mater.* **2000**, *12*, 845−853.
(27) de Moor, P. P. E. A.; Beelen, T. P. M.; van Santen, R. A.; Beck, L. W.; Davis, M. E. *J. Phys. Chem. B* **2000**, *104*, 7600−7611.
(28) Kragten, D.; Fedeyko, J.; Sawant, K.; Rimer, J.; Vlachos, D.; Lobo, R.; Tsapatsis, M. *J. Phys. Chem. B* **2003**, *107*, 10006−10016.
(29) Harris, R. K.; Jones, J.; Knight, C. T. G.; Newman, R. H. *J. Mol. Liq.* **1984**, *29*, 63−74.
(30) Kinrade, S. D.; Knight, C. T. G.; Pole, D. L.; Syvitski, R. *Inorg. Chem.* **1998**, *37*, 4272−4277.
(31) Kinrade, S. D.; Knight, C. T. G.; Pole, D. L.; Syvitski, R. *Inorg. Chem.* **1998**, *37*, 4278−4283.
(32) Fedeyko, J. M.; Rimer, J. D.; Lobo, R. F.; Vlachos, D. G. *J. Phys. Chem. B* **2004**, *108*, 12271−12275.
(33) Harris, R. K.; Knight, C. T. G. *J. Chem. Soc., Faraday Trans. 2* **1983**, *79*, 1525.
(34) Harris, R. K.; Knight, C. T. G. *J. Chem. Soc., Faraday Trans. 2* **1983**, *79*, 1539.
(35) Knight, C. T. G.; Kirkpatrick, R. J.; Oldfield, E. J. *J. Am. Chem. Soc.* **1986**, *108*, 30.
(36) Knight, C. T. G.; Kirkpatrick, R. J.; Oldfield, E. J. *J. Am. Chem. Soc.* **1987**, *109*, 1632.
(37) Allen, M. P.; Tildesley, D. J. *Computer Simulation of Liquids*; Clarendon: Oxford, 1987.
(38) Jorgensen, W. L. *J. Chem. Phys.* **1982**, *77*, 4156.
(39) Luzhkov, V. B.; Österberg, F.; Acharya, P.; Chattopadhyaya, J.; Aqvist, J. *Phys. Chem. Chem. Phys.* **2002**, *4*, 4640−4647.
(40) Foresman, J. B.; Keith, T. A.; Wiberg, K. B.; Snoonian, J.; Frisch, M. J. *J. Phys. Chem.* **1996**, *100*, 16098−16104.
(41) Breneman, C. M.; Wiberg, K. B. *J. Comput. Chem.* **1990**, *11*, 361−373.
(42) Frisch, M. J.; Trucks, G. W.; Schlegel, H. B.; Scuseria, G. E.; Robb, M. A.; Cheeseman, J. R.; Montgomery, Jr., J. A.; Vreven, T.; Kudin, K. N.; Burant, J. C.; Millam, J. M.; Iyengar, S. S.; Tomasi, J.; Barone, V.; Mennucci, B.; Cossi, M.; Scalmani, G.; Rega, N.; Petersson, G. A.; Nakatsuji, H.; Hada, M.; Ehara, M.; Toyota, K.; Fukuda, R.; Hasegawa, J.; Ishida, M.; Nakajima, T.; Honda, Y.; Kitao, O.; Nakai, H.; Klene, M.; Li, X.; Knox, J. E.; Hratchian, H. P.; Cross, J. B.; Bakken, V.; Adamo, C.; Jaramillo, J.; Gomperts, R.; Stratmann, R. E.; Yazyev, O.; Austin, A. J.; Cammi, R.; Pomelli, C.; Ochterski, J. W.; Ayala, P. Y.; Morokuma, K.; Voth, G. A.; Salvador, P.; Dannenberg, J. J.; Zakrzewski, V. G.; Dapprich, S.; Daniels, A. D.; Strain, M. C.; Farkas, O.; Malick, D. K.; Rabuck, A. D.; Raghavachari, K.; Foresman, J. B.; Ortiz, J. V.; Cui, Q.; Baboul, A. G.; Clifford, S.; Cioslowski, J.; Stefanov, B. B.; Liu, G.; Liashenko, A.; Piskorz, P.; Komaromi, I.; Martin, R. L.; Fox, D. J.; Keith, T.; Al-Laham, M. A.; Peng, C. Y.; Nanayakkara, A.; Challacombe, M.; Gill, P. M. W.; Johnson, B.; Chen, W.; Wong, M. W.; Gonzalez, C.; Pople, J. A. *Gaussian 03*, Revision C.02; Gaussian, Inc., Wallingford CT, 2004.
(43) Frenkel, D.; Smit, B. *Understanding Molecular Simulation*; Academic Press: New York, 2001.
(44) Smith, W.; Forester, T. *J. Mol. Graphics* **1996**, *14*, 136.
(45) Wiebcke, M.; Hoebbel, D. *J. Chem. Soc., Dalton Trans.* **1992**, 2451−2455.
(46) Wiebcke, M.; Grube, M.; Koller, H.; Engelhardt, G.; Felsche, J. *Microporous Mater.* **1993**, *2*, 55−63.
(47) Wiebcke, M.; Emmer, J.; Felsche, J. *Microporous Mater.* **1995**, *4*, 149−1587.